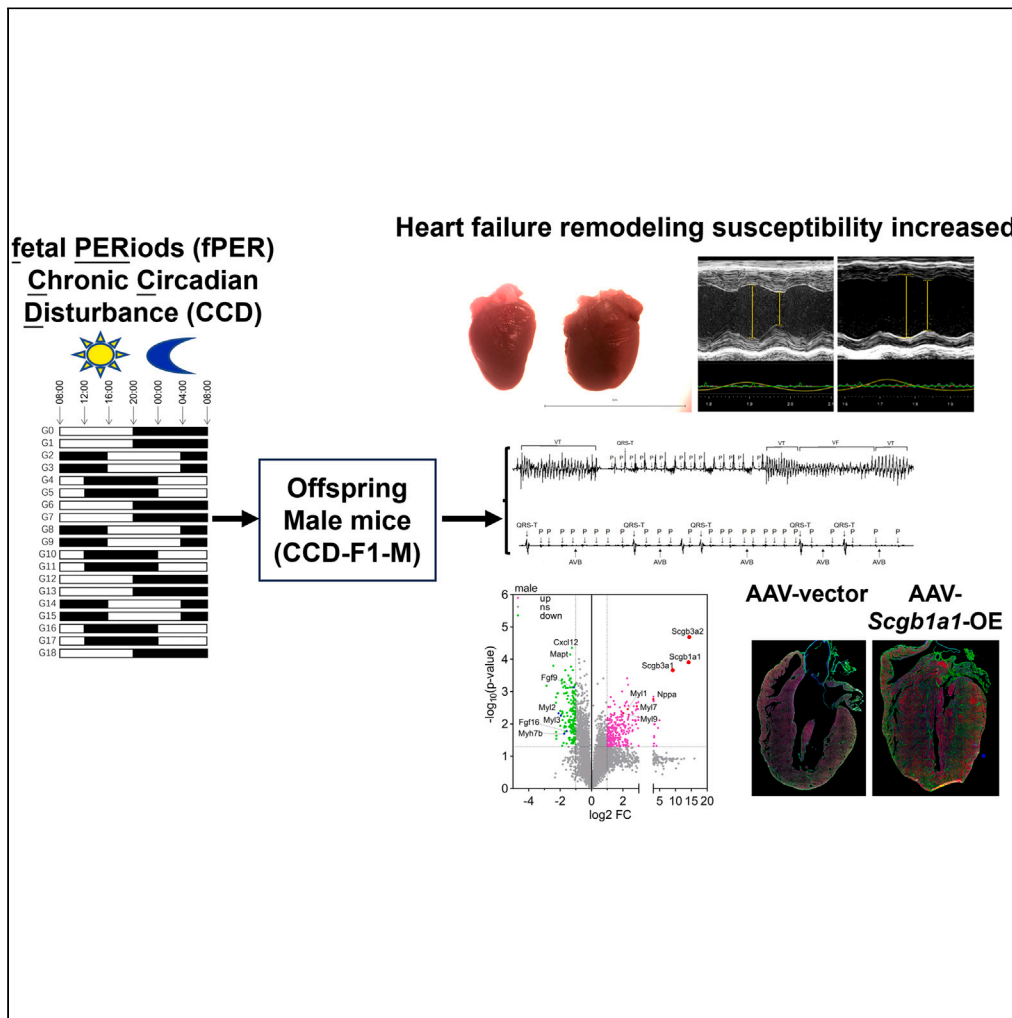


Article

Circadian disruption during fetal development promotes pathological cardiac remodeling in male mice



Yang Yu, Jing-Yu Liu, Hui-Jiao Yang, ..., Hai-Ying Mary Cheng, Wei-Chao Liu, Peng Zhang

haiying.cheng@utoronto.ca (H.-Y.M.C.)
w_liu2019@swmu.edu.cn (W.-C.L.)
zhangpeng@swmu.edu.cn (P.Z.)

Highlights

Circadian disruption *in utero* promotes pathological cardiac remodeling in male mice

Circadian disruption *in utero* sensitizes male mice to ISO-induced tachyarrhythmia

Circadian disruption *in utero* upregulates cardiac *Scgb1a1* expression in male mice

Cardiac overexpression of *Scgb1a1* is sufficient to induce myocardial hypertrophy

Yu et al., iScience 27, 109008
February 16, 2024 © 2024 The Author(s).
<https://doi.org/10.1016/j.isci.2024.109008>



Article

Circadian disruption during fetal development promotes pathological cardiac remodeling in male mice

Yang Yu,^{1,2,5} Jing-Yu Liu,^{1,5} Hui-Jiao Yang,^{1,5} Xiao-Qin Luo,² Xiao-Ping Gao,¹ Xiao-Xin Huang,³ Ao-Xue Tang,³ Hai-Ying Mary Cheng,^{4,*} Wei-Chao Liu,^{1,*} and Peng Zhang^{1,6,*}

SUMMARY

Disruption of circadian rhythms during fetal development may predispose mice to developing heart disease later in life. Here, we report that male, but not female, mice that had experienced chronic circadian disturbance (CCD) *in utero* were more susceptible to pathological cardiac remodeling compared with mice that had developed under normal intrauterine conditions. CCD-treated males showed ventricular chamber dilatation, enhanced myocardial fibrosis, decreased contractility, higher rates of induced tachyarrhythmia, and elevated expression of biomarkers for heart failure and myocardial remodeling. *In utero* CCD exposure also triggered sex-dependent changes in cardiac gene expression, including upregulation of the secretoglobin gene, *Scgb1a1*, in males. Importantly, cardiac overexpression of *Scgb1a1* was sufficient to induce myocardial hypertrophy in otherwise naive male mice. Our findings reveal that *in utero* CCD exposure predisposes male mice to pathological remodeling of the heart later in life, likely as a consequence of SCGB1A1 upregulation.

INTRODUCTION

Like most physiological processes, the cardiovascular system is influenced by the circadian clock, which imparts time-of-day information and organizes physiological processes in synchrony with geophysical time. Heart rate, blood pressure, and cardiac gene expression all exhibit a circadian rhythm.¹ Likewise, the incidence of acute myocardial infarction fluctuates over the 24-h day, peaking between 6:00 a.m. and 12:00 p.m.² A growing body of evidence has demonstrated a reciprocal relationship between circadian disruption and cardiovascular dysfunctions and diseases.^{3,4} Environmental stressors including exposure to light at night, transmeridian travel, and social jetlag can disrupt endogenous circadian rhythms, thereby affecting tissue function and potentially contributing to adverse events leading to cardiovascular diseases.⁵ Just as perturbation of the circadian clock can promote the occurrence and progression of cardiac remodeling,^{6,7} pathological remodeling of the heart can disrupt its inherent daily rhythms, as evident by the abnormal circadian rhythms of heart rate and blood pressure following myocardial infarction or heart failure.^{8,9} In addition, gene manipulation studies in rodents have shown that interfering with the molecular clockwork can impact cardiac structure and function¹⁰ and lead to age-dependent cardiomyopathy.^{6,11,12} Whether or to which extent the circadian clock influences cardiac structure and function in a sexually dimorphic manner remains to be determined.¹³

Given the importance of circadian rhythms to cardiovascular health, a key question that has yet to be addressed is whether chronic circadian disturbance (CCD) during early life (i.e., fetal periods [fPER]) predisposes one to developing heart disease later in life. There is evidence to indicate that CCD during adulthood (e.g., as a result of night-shift work) elevates the risk of cardiovascular diseases.^{14,15} Recently, it has also been shown that prenatal exposure of rats of lipopolysaccharides can induce hypertension that is heritable over several generations.¹⁶ In a previous study, we reported that environmentally induced CCD during pregnancy can lead to sex-specific mood disorders in the first and second filial generations (F1 and F2, respectively).¹⁷ Interestingly, proteins implicated in cardiovascular system development and function represented a major class of differentially expressed proteins in the hypothalamic proteomes of F1 mice exposed to CCD *in utero*, raising the possibility that these mice might also have cardiovascular impairments.

Cardiovascular diseases can occur in both sexes at any age of life,¹⁸ but the published data suggest that there are significant differences between male and female in the occurrence, epidemiology, clinical manifestation, pathophysiology, and outcome of these disorders.^{19,20} The

¹Key Laboratory of Medical Electrophysiology, Ministry of Education & Medical Electrophysiological Key Laboratory of Sichuan Province, (Collaborative Innovation Center for Prevention of Cardiovascular Diseases), Institute of Cardiovascular Research, Southwest Medical University, Luzhou, Sichuan 646000, China

²Department of Human Anatomy and Histoembryology, School of Basic Medical Sciences, Southwest Medical University, Luzhou, Sichuan, China

³School of Basic Medical Science, Southwest Medical University, Luzhou, Sichuan 646000, China

⁴Department of Biology, University of Toronto Mississauga, Mississauga, Ontario L5L 1C6, Canada

⁵These authors contributed equally

⁶Lead contact

*Correspondence: haiying.cheng@utoronto.ca (H.-Y.M.C.), w_liu2019@swmu.edu.cn (W.-C.L.), zhangpeng@swmu.edu.cn (P.Z.)
<https://doi.org/10.1016/j.isci.2024.109008>



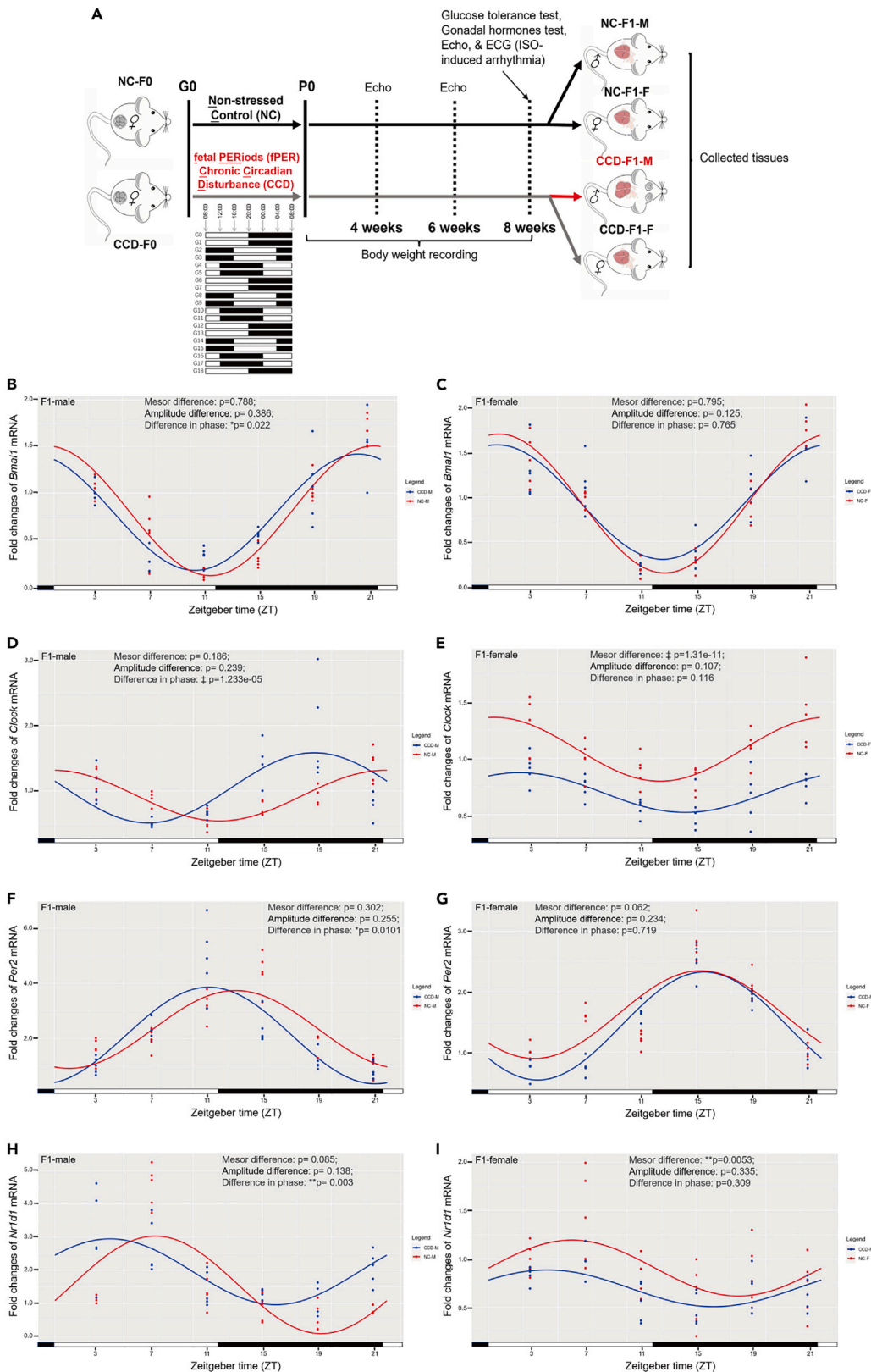


Figure 1. fPER-CCD exposure alters the expression of circadian clock genes in the heart in a sex-dependent manner

(A) Illustration of the experimental design showing the LD cycle changes in the fPER-CCD paradigm and the time course of echocardiography, ECG recording, and collection of serum and tissues.

(B, D, F, H) Cosinor mixed-models of diurnal expression pattern of *Bmal1*, *Clock*, *Per2*, and *Nr1d1*(*Rev-erba*) in the hearts of CCD-F1-M mice (n = 5/ZT/group).

(C, E, G, I) Diurnal expression pattern of *Bmal1*, *Clock*, *Per2*, and *Nr1d1* in the hearts of CCD-F1-F mice (n = 5/ZT/group). Statistical significance is determined by cosinor analysis. *p < 0.05, **p < 0.01, ‡p < 0.00001 vs. sex- and age-matched NC-F1 controls.

incidence of some cardiovascular disorders is typically higher in males compared with age-matched females.²¹ However, the prognosis for females tends to be poorer, given the later onset of these diseases in older, post-menopausal women, e.g., in coronary artery disease.²² It is well established that premenopausal women have a lower incidence of coronary artery disease, myocardial infarction, and left-ventricular hypertrophy, as well as decreased cardiac remodeling compared with their age-matched males.^{23–25} However, sexual differences in circadian-rhythm-induced cardiac remodeling have not been fully elucidated. In the current study, we set out to determine whether *in utero* CCD exposure predisposed mice to developing cardiac disease later in life in a sex-dependent fashion and if so, to identify the potential molecular substrates of CCD that may trigger or mediate pathological changes in the heart.

RESULTS**Exposure to chronic circadian disturbance during the fetal PERiod influences body weight gain, glucose metabolism, and sex hormone levels in a sex-specific fashion**

To achieve fPER-CCD, pregnant females (F0 generation) were maintained on a 12-h light:12-h dark cycle that was delayed by 8 h once every two days (Figure 1A).^{26,27} F0 females were housed under these conditions from gestation day 0 (G0) to the day of birth (postnatal day 0 [P0]). We and others have used repeated 8-h delays of the LD cycle to disrupt circadian clock gene expression in rodents.^{17,26,28} In our previous studies, we showed to this particular fPER-CCD protocol perturbed *Bmal1*, *Clock*, *Per1*, and *Per2* mRNA rhythms in the SCN and ovaries of F1 adult offspring, thereby validating the effectiveness of this protocol to induce circadian disruption.^{17,28}

To determine whether *in utero* exposure to CCD affects the physical development of mice, we tracked their body weights from weaning to 8 weeks of age. Three-week-old F1 male and female mice that had been exposed to fPER-CCD (CCD-F1-M and CCD-F1-F, respectively) weighed significantly less than their same-sex counterparts that had developed under normal conditions *in utero* (NC-F1-M and NC-F1-F) (Figure S1A). Subsequent weight gain of CCD-F1-M mice was accelerated compared with NC-F1-M controls. CCD-F1-M mice were significantly heavier than controls at 8 weeks of age, although the body weights of both male groups across all ages were not significantly different when analyzed by two-way ANOVA (Figure S1A). CCD-F1-F mice were significantly lower in body weight than NC-F1-F controls from 3 to 7 weeks of age (Figure S1B).

Next, we examined the glucose tolerance of 8-week-old CCD-F1 and NC-F1 mice after a 12-h fast (Figures S1C and S1D). CCD-F1-F mice were indistinguishable from NC-F1-F controls in terms of their blood glucose concentration under fasted conditions, both before and after glucose challenge (Figure S1D). In contrast, CCD-F1-M mice exhibited elevated blood glucose concentration prior to glucose challenge (t = 0) and a lower peak 15-min post-challenge compared with NC-F1-M controls (Figure S1C).

In addition, we compared the levels of serum circulating gonadal hormones between 8-week-old CCD-F1 and NC-F1 mice. Whereas CCD-F1-M and NC-F1-M mice had similar levels of free testosterone (Figure S1E), CCD-F1-F mice had significantly reduced estradiol levels compared with NC-F1-F controls (Figure S1F). Collectively, our data suggest that fPER-CCD exposure affects body weight gain, response to glucose challenge, and gonadal hormone levels in offspring mice in a sex-dependent manner.

fPER-CCD exposure leads to sex-dependent disruption of circadian clock gene expression in the heart

To determine the effects of fPER-CCD exposure on the cardiac circadian clock, we examined circadian clock gene expression in the heart at six Zeitgeber times (ZT) spanning a 24-h interval. Four genes were assessed by qRT-PCR: the positive regulators, *Bmal1* and *Clock*, and the negative regulators, *Per2* and *Nr1d1* (*Rev-erba*). Cosinor analysis revealed that *Bmal1*, *Clock*, *Per2*, and *Nr1d1* mRNA rhythms were phase-advanced in the hearts of CCD-F1-M mice relative to NC-F1-M controls (Figures 1B–1D, 1F, and 1H). For the abovementioned genes, mesor and amplitude were not significantly different between the two groups of male mice. In contrast, the phase and amplitude of *Bmal1*, *Clock*, *Per2*, and *Nr1d1* rhythms were similar between CCD-F1-F and NC-F1-F mice, although fPER-CCD reduced the mesor of *Clock* and *Nr1d1* expression in the female heart (Figures 1C–1E, 1G, and 1I). Our results suggest that fPER-CCD has a more disruptive effect on clock gene rhythms in the hearts of male offspring compared with females.

CCD-F1-M mice exhibit heart-failure-like left ventricular remodeling

Next, we asked whether perturbed circadian clock gene expression in the hearts of CCD-F1 mice is accompanied by structural and functional changes. Based on morphological and histological analyses, 8-week-old CCD-F1-M mice exhibited a larger diameter along the short axis of the heart, a reduced heart-to-body-weight ratio, ventricular chamber dilatation, wall thinning, and cardiac apex passivation compared with NC-F1-M controls (Figures 2A–2C). In contrast, there were no obvious morphological differences between CCD-F1-F and NC-F1-F mice (Figures 2A–2C).

To evaluate heart function, we performed echocardiography on all groups of F1 mice at 4, 6, and 8 weeks of age. Compared with NC-F1-M mice, CCD-F1-M mice exhibited ventricular wall thinning along with an increase in the ventricular diameter (Figure 2D). In addition, left

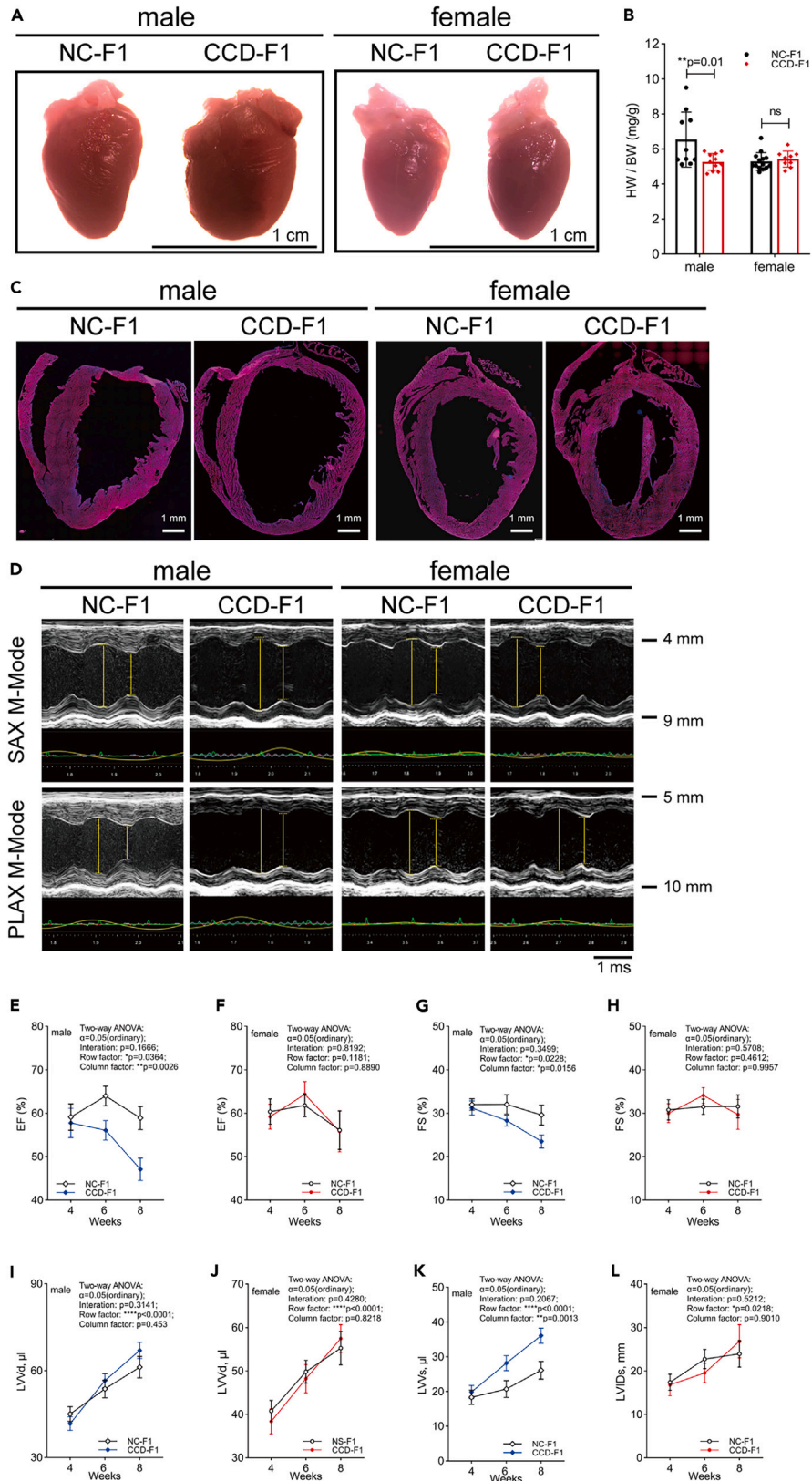


Figure 2. fPER-CCD exposure alters cardiac morphology and function in a sex-dependent manner

(A) Representative image of freshly dissected hearts from 8-week-old NC-F1 and CCD-F1 mice.
(B) Heart-to-body weight (HW/BW, mg/g) ratios of CCD-F1 and NC-F1 mice.
(C) Immunofluorescent staining of coronal sections of the whole heart. Red: α -ACTIN; Blue: DAPI.
(D) Representative M-mode echocardiographic images from the parasternal long axis (PSLAX) and short axis (SAX) views. The images show LV chamber dilatation and LV wall myocardium thinning.
(E and F) LV ejection fraction (EF, %) in 4-, 6-, and 8-week-old mice.
(G and H) LV fractional shortening (FS, %) in 4-, 6-, and 8-week-old mice.
(I and J) LV volume at diastole (LVVd) in 4-, 6-, and 8-week-old mice.
(K and L) LV volume at systole (LVVs) in 4-, 6-, and 8-week-old mice. Statistical significance is determined by two-way ANOVA, * $p < 0.05$, ** $p < 0.01$, **** $p < 0.0001$ vs. sex- and age-matched NC-F1 groups. $n = 19$ (NC-F1-M), 17 (CCD-F1-M), 22 (NC-F1-F), and 18 (CCD-F1-F).

ventricular (LV) ejection fraction (EF) and LV fractional shortening (FS) were significantly reduced in CCD-F1-M mice relative to NC-F1-M controls at 6 and 8 weeks of age (Figures 2E and 2G). CCD-F1-M mice exhibited a greater LV volume at systole (LVVs) (Figure 2K) but no difference in LV volume at diastole (LVVd) (Figure 2I), compared with NC-F1-M controls. CCD-F1-F and NC-F1-F mice were similar in most echocardiographic parameters at all ages examined (Table 1; Tables S3 and S4). Collectively, our data suggest that fPER-CCD exposure triggers heart-failure-like LV remodeling in male but not female offspring.

CCD-F1-M mice exhibit increased incidence of arrhythmias and cardiac arrest

To determine whether fPER-CCD alters the electrophysiological properties of the heart, we performed electrocardiogram (ECG) recordings on CCD-F1 and NC-F1 mice before and after an intraperitoneal injection of isoprenaline (ISO). A low (10 μ g/kg) and a high (100 μ g/kg) dose of ISO were evaluated for their ability to induce various types of cardiac arrhythmias, including premature ventricular contraction/complex (PVC and Salvo), atrioventricular block (AVB), ventricular tachycardia (VT), ventricular fibrillation (VF), and heart arrest. At the low ISO dose, severe arrhythmic events (i.e., VT and VF) were observed only in the CCD-F1-M group, but their incidence rates were nevertheless statistically indistinguishable from those of NC-F1-M controls (Table S5). In contrast, at the high ISO dose, CCD-F1-M mice had a significantly greater incidence of severe arrhythmic events and a higher mortality rate compared with NC-F1-M controls (Figures 3B and 3E; Table 2). CCD-F1-F and NC-F1-F mice were statistically similar in their response to both doses of ISO, even though 5 out of 29 CCD-F1-F mice did exhibit AVB, VT, and/or VF at the higher dose (Tables 2 and S5).

All experimental groups displayed normal sinus rhythms under baseline conditions. Under isoflurane gas anesthesia, all mice exhibited uniform heart rates and regular QRST and P waves (Figures 3A–3D). Within 20 min of high-dose ISO injection, 47% of CCD-F1-M mice exhibited VT and/or VF; in some cases, VT/VF alternated with normal sinus rhythms (Figure 3B), whereas in others, VF was permanent (Figure 3B-2). By comparison, only 11%–15% of NC-F1-M mice exhibited VT and/or VF (Table 2). Approximately 22% of CCD-F1-M mice developed complete AVB (Figures 3B–3I), all of which ended in cardiac arrest. In contrast, CCD-F1-F mice had a significantly lower incidence of severe arrhythmic events and reduced mortality rates compared with CCD-F1-M mice (Figures 3C and 3D; Table 2). Altogether, our data show that fPER-CCD increases the susceptibility of male, but not female, mice to cardiac arrhythmias.

CCD-F1-M mice exhibit elevated expression of molecular markers of cardiac remodeling

Next, we investigated the effects of fPER-CCD exposure on the expression of molecular markers of cardiac remodeling and fibrosis. Immunofluorescence staining revealed elevated expression of type 3A1 collagen protein (COL3A1) in the hearts of CCD-F1-M mice relative to other groups (Figures 4A and 4B). Sirius Red staining indicated that CCD-F1-M had larger fibrotic areas (red zone) containing type I and III collagen fibers in the interstitium between myocardial fibers when compared with NC-F1-M controls and both female groups (Figures 4C and 4D). The following proteins were upregulated in the hearts of CCD-F1-M mice relative to NC-F1-M controls: brain natriuretic peptide (BNP) (Figures 4E and 4F), a marker of increased myocardial wall tension; tumor necrosis factor alpha (TNF- α) (Figures 4E and 4F) and matrix metalloproteinase 2 (MMP2) (Figures 4I and 4J), markers of fibrosis; tyrosine hydroxylase (TH) (Figures 4I and 4J), a marker of cardiac sympathetic nerves; and alpha-actin (α -ACTIN) (Figures 4E and 4F), a marker of myocardial injury. With the exception of α -ACTIN, none of these proteins were significantly altered in their expression in the hearts of CCD-F1-F mice when compared with NC-F1-F controls (Figures 4G, 4H, 4K, and 4L). Collectively, our data reveal that fPER-CCD exposure upregulates the expression of proteins normally associated with cardiac remodeling in the hearts of male but not female mice.

CCD-F1 mice exhibit sex-specific differential gene expression in the heart

Next, we investigated the impact of fPER-CCD exposure on the cardiac transcriptome of adult offspring by RNA-seq, with the goal of identifying potential candidate genes responsible for fPER-CCD-induced pathological LV remodeling. We harvested the hearts of CCD-F1-M and CCD-F1-F mice that exhibited severe arrhythmic events (AVB, VT, VF) in response to high-dose ISO at the end of the electrocardiogram (ECG) session, at \sim ZT 2. They were compared with same-treated NC-F1-M and NC-F1-F mice that showed normal sinus rhythms, harvested also at \sim ZT 2. We opted to use ISO-treated mice rather than naive mice for RNA-seq analysis, because we wanted to use ECG as a screening tool to minimize inter-sample variability within treatment groups, as not all CCD-F1-M mice developed cardiac impairments (Figure 3; Table 2). There were 473 DEGs in the CCD-F1-M group, of which 305 and 168 were up- and downregulated, respectively (Figure 5A; Table S6). By comparison, the CCD-F1-F group had 111 up- and 246 downregulated genes, for a total of 357 DEGs (Figure 5A; Table S6). The vast majority of

Table 1. M-mode echocardiographic parameters in 8-week-old CCD-F1 and NC-F1 mice of both sexes

	NC-F1-M (N = 19)	CCD-F1-M (N = 17)	p value (NC-F1-M vs. CCD-F1-M)	NC-F1-F (N = 22)	CCD-F1-F (N = 18)	p value (NC-F1-F vs. CCD-F1-F)	p value (NC-F1-M vs. NC-F1-F)	p value (CCD-F1-M vs. CCD-F1-F)
	AVG (SD)	AVG (SD)		AVG (SD)	AVG (SD)			
LVAWd (mm)	0.85 (±0.171)	0.86 (±0.089)	0.869	0.78 (±0.122)	0.71 (±0.091)	0.698	0.190	**0.009
LVAWs (mm)	1.19 (±0.203)	1.16 (±0.176)	0.650	1.11 (±0.177)	1.03 (±0.121)	0.944	0.221	0.313
IVSd (mm)	0.84 (±0.140)	0.80 (±0.113)	0.523	0.79 (±0.108)	0.71 (±0.094)	0.624	0.243	0.340
IVSs (mm)	1.21 (±0.217)	1.13 (±0.186)	0.316	1.17 (±0.239)	1.04 (±0.154)	0.481	0.669	0.799
LVIDd (mm)	3.84 (±0.216)	3.92 (±0.267)	0.287	3.59 (±0.414)	3.41 (±0.302)	0.614	0.054	*0.030
LVIDs (mm)	2.67 (±0.364)	3.02 (±0.306)	*0.002	2.49 (±0.574)	2.45 (±0.607)	0.615	0.326	*0.026
LVPWd (mm)	0.75 (±0.127)	0.72 (±0.084)	0.569	0.75 (±0.116)	0.59 (±0.101)	**0.009	0.977	*0.013
LVPWs (mm)	1.10 (±0.232)	0.93 (±0.112)	*0.012	1.08 (±0.215)	0.84 (±0.205)	*0.0433	0.772	0.557
EF (%)	58.89 (±10.262)	46.14 (±10.202)	***0.00062	59.19 (±12.763)	53.51 (±15.554)	0.654	0.944	*0.039
FS (%)	31.08 (±7.388)	22.92 (±5.950)	***0.00083	31.58 (±9.874)	28.34 (±11.798)	0.944	0.878	0.056
LVVd (μL)	61.21 (±14.349)	70.00 (±11.279)	0.176	55.26 (±14.408)	53.91 (±11.04)	0.667	0.275	*0.034
LVSs (μL)	26.11 (±9.903)	36.06 (±8.703)	**0.002	23.92 (±11.425)	25.79 (±13.178)	0.551	0.585	*0.035
SV (μL)	35.10 (±7.379)	30.93 (±9.280)	0.164	31.33 (±5.276)	28.62 (±4.365)	0.721	0.127	0.919

Left ventricular (LV) internal dimensions at diastole (LVIDd) and systole (LVIDs). LV posterior wall dimensions at diastole (LVPWd) and systole (LVPWs). LV fractional shortening (FS, %) and LV ejection fraction (EF, %). LV volume at diastolic (LVVd) and systole (LVSs). Stroke volume (SV). Statistical significance is analyzed by two-tailed unpaired Student's t test, *p < 0.05, **p < 0.01, ***p < 0.001.

Table 2. Arrhythmia induced by ISO (100 µg/kg, i.p.) in 8-week-old CCD-F1 and NC-F1 mice of both sexes

	ISO (100 µg/kg, i.p.)		p value (NC-F1-M vs. CCD-F1-M)	NC-F1-F (N = 25)	CCD-F1-F (N = 29)	p value (NC-F1-F vs. CCD-F1-F)	p value (NC-F1-M vs. NC-F1-F)	p value (CCD-F1-M vs. CCD-F1-F)
	NC-F1-M (N = 26)	CCD-F1-M (N = 32)						
Normal (%)	11 (42.31%)	6 (18.75%)	0.095	16 (64%)	15 (51.72%)	0.526	0.204	*0.015
PVC (%)	14 (53.85%)	25 (78.13%)	0.093	9 (36%)	12 (41.38%)	0.901	0.318	**0.008
AVB (%)	2 (7.69%)	7 (21.88%)	0.263	2 (8%)	3 (10.34%)	0.862	0.631	0.385
VT (%)	4 (15.38%)	14 (43.75%)	*0.042	0 (0%)	2 (6.90%)	0.538	0.128	**0.003
VF (%)	3 (11.54%)	15 (46.88%)	**0.009	0 (0%)	2 (6.90%)	0.538	0.248	**0.001
VT/VF rate (%)	4 (15.38%)	15 (46.88%)	*0.024	0 (0%)	4 (13.79%)	0.159	0.128	*0.012
Survival rate (%)	24 (92.31%)	21 (65.63%)	*0.035	25 (100%)	27 (93.10%)	0.538	0.488	*0.021

Significance is analyzed by Chi-square statistics (χ^2 test), *p < 0.05, **p < 0.01.

DEGs were not shared between the CCD-F1-M and CCD-F1-F groups (Figures 5A and 5B). The exceptions are six genes that were downregulated (*myl3*, *myh7b*, *Bdh1*, *Mapt*, *Hand2*, and *Sik1*) and 12 genes that were upregulated in both sexes (Figure 5A). In addition, there are 18 genes that were upregulated in CCD-F1-M mice but downregulated in CCD-F1-F mice and one gene (*Adamts4*) that was downregulated in CCD-F1-M mice but upregulated in CCD-F1-F mice (Figure 5A). Chromosomes 1, 14, 17, 18, and X exhibited sex differences in the number of DEGs: except for chromosome 18, there were more DEGs on these chromosomes in CCD-F1-M mice than in CCD-F1-F animals (Figure 5C).

Gene Ontology (GO) enrichment analysis of the DEGs also revealed sex differences. "Myofibril" and "muscular system processes" were the two most enriched GO terms in the CCD-F1-M group (Figure 5D). In CCD-F1-F mice, "fat cell differentiation" and "mitochondrial protein complex" were the most enriched GO terms in the set of up- and downregulated DEGs, respectively (Figure 5D).

Protein interaction (PPI) networks were constructed using the DEGs from the CCD-F1-M and CCD-F1-F groups, considered together (Figure 5E) or independently (Figures S4A–S4D). "Contractile fiber/myosin complex/myofibril" was one of the largest PPI networks in both sexes of CCD-F1 mice (Figure 5E); interestingly, the DEGs of this network were mainly upregulated in CCD-F1 males but downregulated in the females. Additionally, in CCD-F1-M mice, the upregulated DEGs were enriched for the GO terms "actin cytoskeleton," "ionotropic glutamate receptor complex," "metabolism of xenobiotics by cytochrome," and "blood circulation" (Figure S4A), whereas the downregulated DEGs were enriched for the terms "myofibril" and "regulation of metal ion transport" (Figure S4C). By comparison, in CCD-F1-F mice, the upregulated DEGs were enriched for the GO term "fat cell differentiation" (Figure S4B), whereas the downregulated DEGs were enriched for the terms "respiratory chain complex I," "cytosolic ribosome," and "motor activity" (Figure S4D). qPCR analyses of select DEGs were largely consistent with, and thus validated, the RNA-seq results (Figures S4E and S4F). Overall, our data suggest that fPER-CCD exposure alters the transcriptional landscape in the hearts of adult offspring in a sexually dimorphic manner.

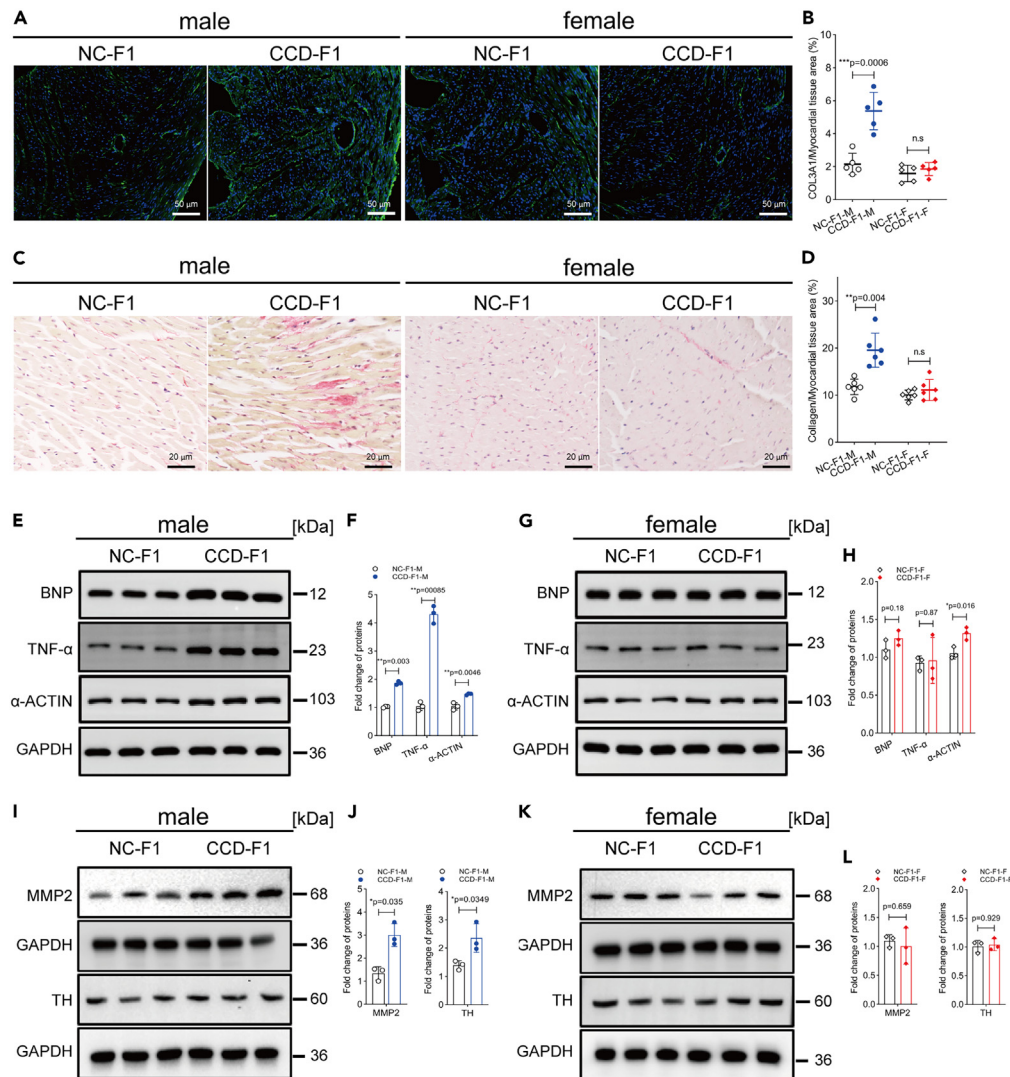
CCD-F1-M mice exhibit aberrantly high expression of the secretoglobin family genes in the heart

To identify potential causal genes of pathological LV remodeling, we constructed volcano plots with the set of DEGs (Figures 6A and 6B). Relative to NC-F1-M controls, CCD-F1-M mice exhibited a consistent, large, and statistically significant increase in the expression of three secretoglobin (SCGB) genes: *Scgb1a1*, *Scgb3a1*, and *Scgb3a2* (Figure 6A). Even though these genes also appeared to be elevated in CCD-F1-F mice compared with NC-F1-F controls, we detected no significant difference between the two groups due to the highly variable expression in CCD-F1-F mice (Figure 6B). The expression of *Scgb1a1*, *Scgb3a1*, and *Scgb3a2* in the hearts of parental females (NC-F0-F and CCD-F0-F) and their offspring (NC-F1-F, CCD-F1-F, NC-F1-M, and CCD-F1-M) were further evaluated by qRT-PCR. All three SCGBs were significantly upregulated in the hearts of CCD-F1-M mice relative to NC-F1-M controls, with *Scgb1a1* and *Scgb3a2* exhibiting substantially larger fold change compared with *Scgb3a1* (Figures 6C–6E). In line with the RNA-seq results, the expression of these SCGBs was variable in F0 and F1 CCD female mice and was not significantly different from corresponding NC-F groups (Figures 6C–6E).

To evaluate whether the change in SCGB expression is specific to the heart, we examined SCGB protein abundance in the hearts and lungs of NC-F1 and CCD-F1 mice (Figures 6F–6H). Levels of SCGB1A1 and SCGB3A2, but not SCGB3A1, were upregulated in the hearts of CCD-F1-M mice compared with NC-F1-M controls (Figures 6F and 6G). In contrast, the lungs of CCD-F1-M mice had similar expression of SCGB1A1 and SCGB3A1, and higher expression of SCGB3A2, when compared with NC-F1-M mice (Figures 6F and 6G). *Scgb1a1* transcript levels were similar in the lungs of CCD-F1-M and NC-F1-M mice (Figure 6H). Collectively, these data indicate a heart-specific increase in *Scgb1a1* expression at the transcript and protein levels in male offspring previously exposed to fPER-CCD.

Overexpression of SCGB1A1 induces myocardial hypertrophy in mice

To determine whether the upregulation of cardiac SCGB1A1 in CCD-F1-M mice is causal to LV remodeling, we overexpressed SCGB1A1 in the myocardium of C57BL/6J male mice using an AAV gene delivery approach. The AAV2-*cTnt-Scgb1a1*-3×flag-*mCherry* (AAV-*Scgb1a1*-OE)



vector expresses *Scgb1a1* and FLAG-tagged mCherry under the control of the cardiomyocyte-specific *cTNT* promoter (Figure S6). Six weeks after multi-point intramyocardial injection of AAV-*Scgb1a1*-OE, we were able to detect a ~150-fold increase in *Scgb1a1* transcript and a ~3-fold increase in SCGB1A1 protein in the hearts of these animals relative to controls that had been injected with AAV-*cTNT*-mCherry (AAV-vector) (Figures 7A–7D). Given that SCGB1A1 is a secreted, cytokine-like protein,²⁶ it is not wholly unexpected that protein accumulation within heart tissue is more modest when compared with transcript abundance. Along these lines, we also found that serum SCGB1A1 levels were increased by ~2.5-fold in AAV-*Scgb1a1*-OE mice (Figure 7E).

AAV-*Scgb1a1*-OE mice were similar to AAV-vector control mice in terms of body weight (Figure 7F). However, the heart-to-body-weight ratio was significantly greater in AAV-*Scgb1a1*-OE mice, indicating that the hearts were enlarged (Figure 7G). Importantly, myocardial hypertrophy and left ventricular stenosis were evident from long-axis tissue sections of the hearts of AAV-*Scgb1a1*-OE mice and were not observed in AAV-vector control animals (Figure 7A). AAV-*Scgb1a1*-OE mice also exhibited increased cardiac expression of COL3A1, a marker of cardiomyocyte hypertrophy (Figures 7A–7I). M-mode echocardiograms from the SAX and PLAX views revealed significant thickening of the left

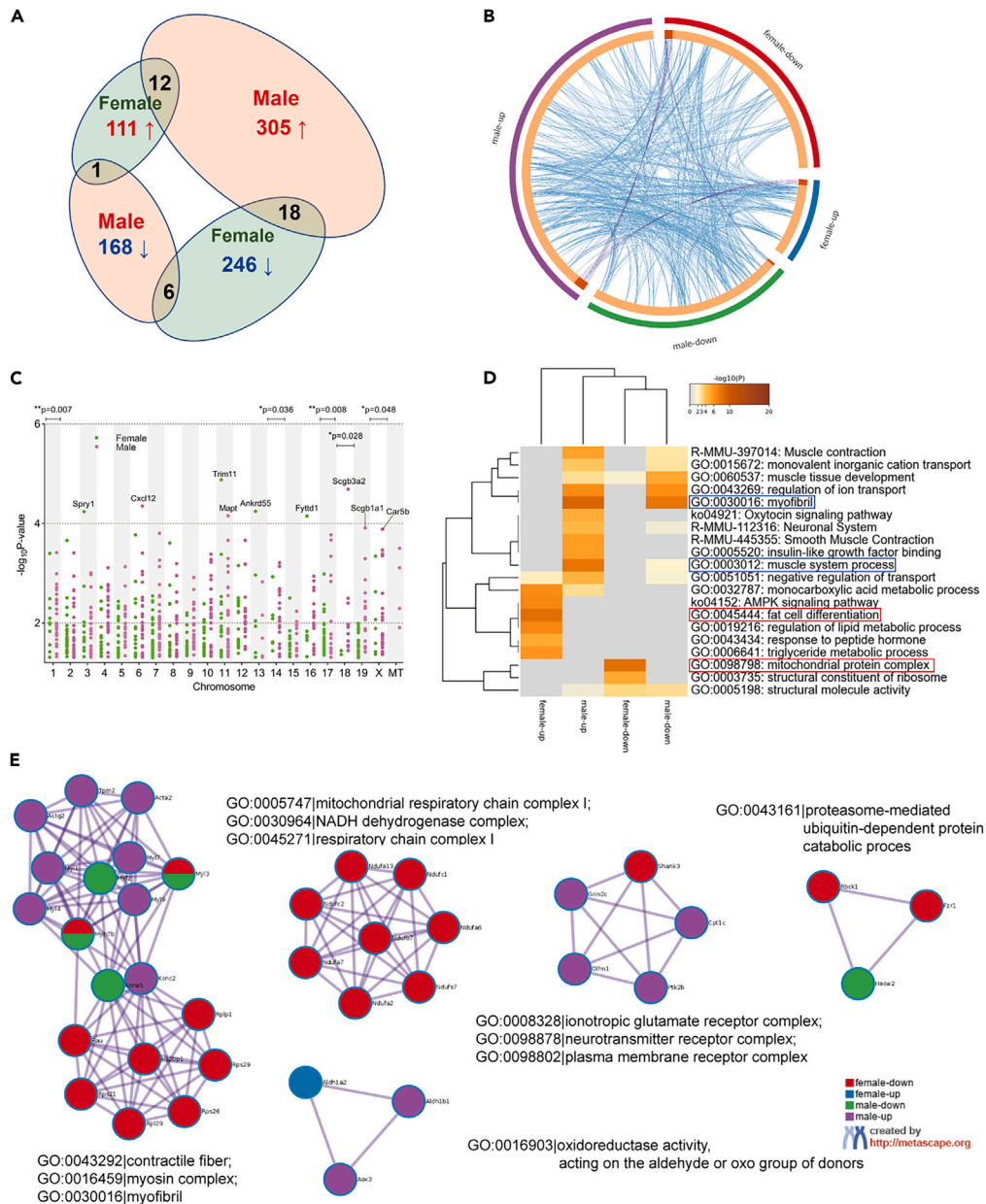


Figure 5. fPER-CCD triggers sex-specific differential gene expression in the heart

(A) Venn diagram showing the overlap between up- and downregulated DEGs in CCD-F1-M and CCD-F1-F mice.

(B) Circos plot of the up- and downregulated DEGs from the hearts of CCD-F1-M and CCD-F1-F mice. Arcs of the outer ring represent the four DEG lists. Each gene occupies a unique spot on one or more arcs of the inner ring. Dark orange regions of the inner arcs represent genes that appear in multiple DEG lists, and light orange regions of the inner arcs represent genes that are unique to a particular DEG list. Purple lines link the same genes that are shared by multiple DEG lists. Blue lines link different genes that share the same significantly enriched GO term. More purple links and longer dark orange arcs indicate greater overlap among the DEG lists. Blue links indicate the amount of functional overlap among the DEG lists.

(C) Visualization of DEGs using the Manhattan plot. Each point represents a DEG that fulfilled the following conditions: log₂ fold changes >1, log₂ fold changes < -1, and p-value <0.05. Points were plotted with the chromosomal position along the x axis and the negative logarithm of the associated p-value along the y axis. Red and green dots represent DEGs in CCD-F1-M and CCD-F1-F mice, respectively.

(D) Heatmap of up- and downregulated DEGs in CCD-F1-M and CCD-F1-F mice by GO enrichment analysis.

(E) The top 5 protein-protein interaction (PPI) networks identified from the up- and downregulated DEGs in CCD-F1-M and CCD-F1-F mice. Downregulated DEGs in CCD-F1-F mice (red); upregulated DEGs in CCD-F1-F mice (blue); downregulated DEGs in CCD-F1-M mice (green); upregulated DEGs in CCD-F1-M mice (purple). Statistical significance is determined by two-tailed unpaired Student's t tests, *p < 0.05, **p < 0.01 vs. NC-F1 group (n = 3/group).

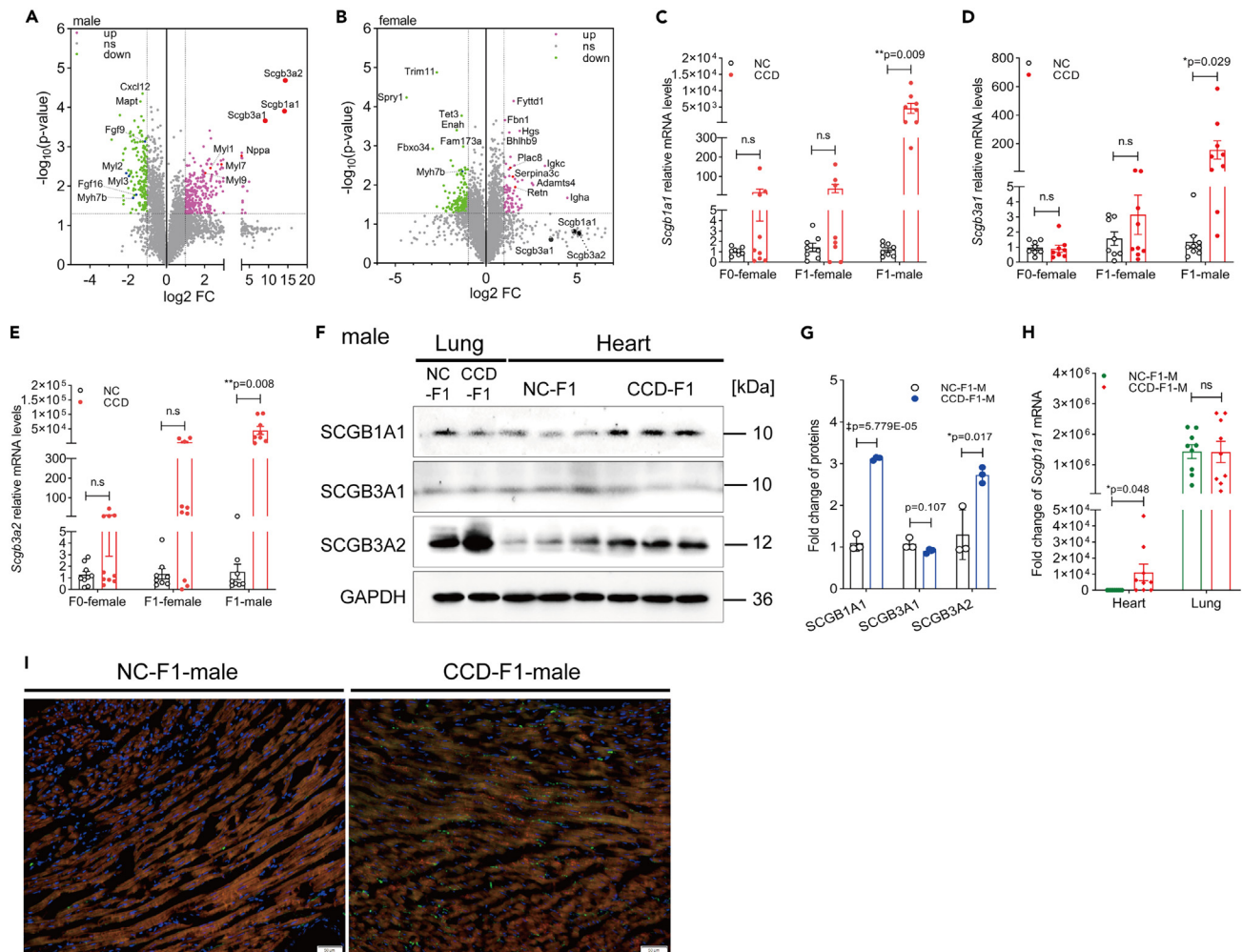


Figure 6. CCD-F1-M mice have aberrantly high expression of SCGBs in the heart

(A and B) Volcano plots of DEGs detected in the hearts of CCD-F1-M (A) and CCD-F1-F mice (B). Green dots represent significantly downregulated DEGs with $\log_2 FC < -1$ and $-\log_{10}(p \text{ value}) > 1.3$. Pink dots represent significantly upregulated DEGs with $\log_2 FC > 1$ and $-\log_{10}(p \text{ value}) > 1.3$.

(C–E) RT-qPCR analysis of *Scgb1a1* (C), *Scgb3a1* (D), and *Scgb3a2* (E) transcript levels in the hearts of F0 and F1 generations of CCD and NC mice, expressed as fold change relative to the NC-F0-F group. (n = 8–10/group).

(F) Western blot analysis of SCGB1A1, SCGB3A1, and SCGB3A2 proteins in the hearts and lungs of NC-F1-M and CCD-F1-M mice.

(G) Semi-quantitative measurements of SCGB1A1, SCGB3A1, and SCGB3A2 protein abundance in the hearts of CCD-F1-M and NC-F1-M mice, expressed as fold change relative to the NC-F1-M group. (n = 3/group).

(H) RT-qPCR analysis of *Scgb1a1* transcript levels in the lungs of CCD-F1-M and NC-F1-M mice, expressed as fold change relative to the NC-F1-M group (n = 8–10/group).

(I) Immunofluorescence detection of SCGB1A1 (red) and TH (green) in the hearts of NC-F1-M and CCD-F1-M mice. SCGB1A1 exhibits a characteristic cytoplasmic punctate distribution, evident in CCD-F1-M samples. Blue indicates DAPI. Statistical significance is determined by two-tailed unpaired Student's t tests or the Mann–Whitney test (G). *p < 0.05, **p < 0.01, ‡p < 0.0001 vs. sex-matched NC-F1 group. n.s., not significant.

ventricular muscle layer six weeks after AAV-*Scgb1a1* injection but not after AAV-vector control injection (Figures 7J and 7K). LV ejection fraction (EF%) was reduced in the weeks following AAV-*Scgb1a1* injection, reaching statistical significance at six weeks post-injection (Figure 7L). Collectively, our results show that upregulation of cardiac SCGB1A1 is sufficient to induce myocardial remodeling.

DISCUSSION

In the present study, we show that chronic circadian disruption during fetal development has a profound impact on cardiac health later in life, especially in male mice. fPER-CCD exposure triggers pathological remodeling of the heart, compromises cardiac electrical activity and systolic function, and increases the susceptibility of mice to cardiac arrhythmia and arrest. To our knowledge, we are the first to demonstrate that early-life circadian disruption can predispose one to pathological cardiac remodeling later in life. We further show that fPER-CCD leads to an

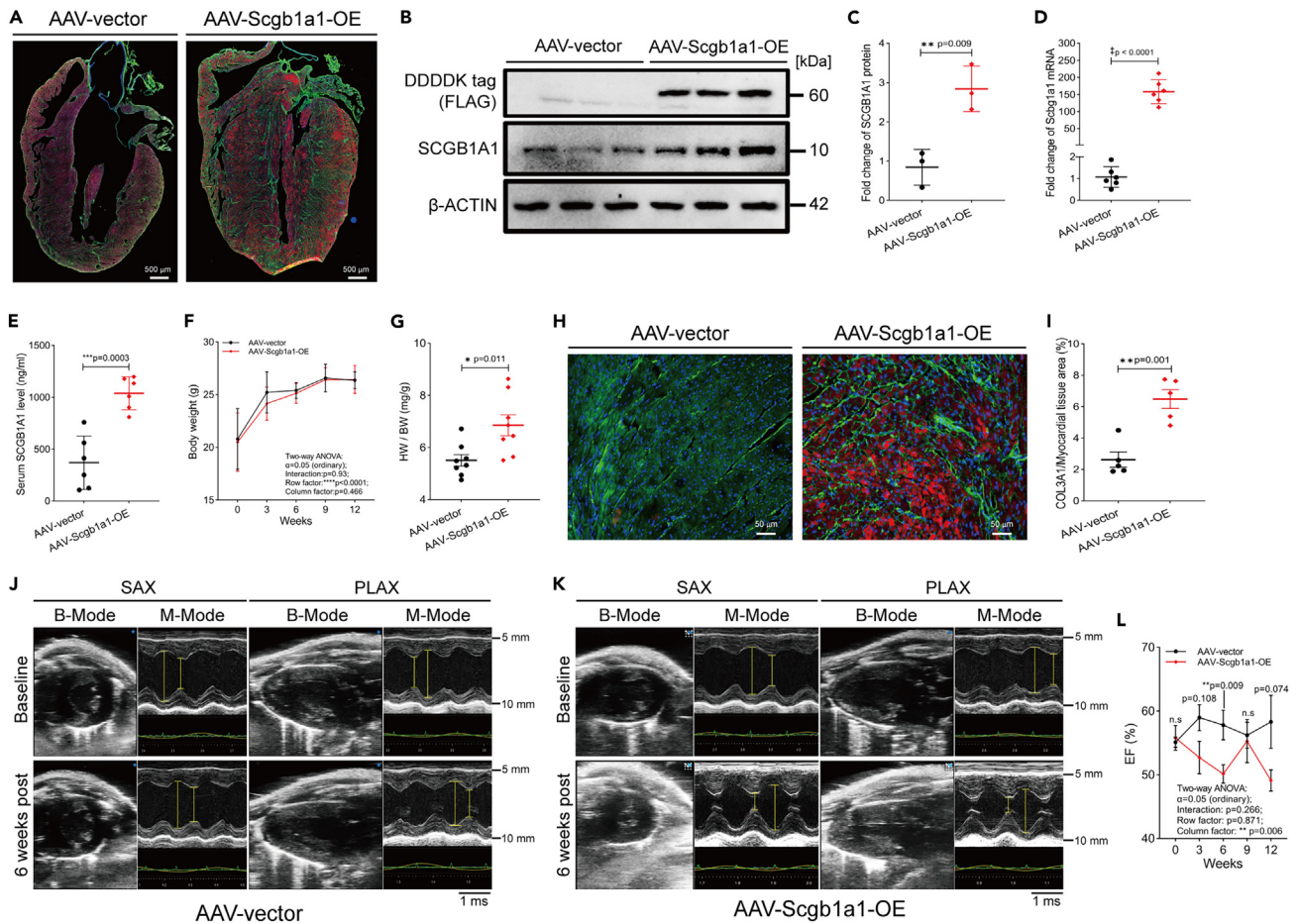


Figure 7. Overexpression of *Scgb1a1* in the heart is sufficient to induce myocardial hypertrophy in naive male mice that had developed under normal conditions in utero

(A) Representative photomicrographs of immunostained hearts from C57Bl6/J male mice that had been injected intracardially with AAV-vector (control) or AAV-*Scgb1a1*-OE. COL3A1 (green); 3x-FLAG-mCherry (red); DAPI (blue).
 (B) Western blot analysis of 3xFLAG-mCherry and SCGB1A1 expression in the heart, six weeks post-injection with AAV-*Scgb1a1*-OE or AAV-vector control. Note that the mCherry protein expressed by the control vector does not contain the FLAG tag. β -ACTIN was used as the loading control.
 (C) Semi-quantitative measurements of SCGB1A1 protein levels, expressed as fold-change relative to AAV-vector control.
 (D) RT-qPCR analysis of *Scgb1a1* transcript levels in the heart, six weeks post-injection with *Scgb1a1*-OE or AAV-vector control.
 (E) Serum levels of SCGB1A1 by ELISA.
 (F) Body weights of male mice injected with AAV-*Scgb1a1*-OE or AAV-vector control, at 0, 3, 6, 9, and 12 weeks after AAV injection.
 (G) Heart-to-body weight (HW/BW, mg/g) ratios of mice injected with AAV-*Scgb1a1*-OE or AAV-vector control.
 (H) Immunofluorescence detection of COL3A1 (green) in the heart, six weeks post-injection with AAV-*Scgb1a1*-OE or AAV-vector control. 3x-FLAG-mCherry (red); DAPI (blue).
 (I) Ratio of COL3A1-stained area in the LV and myocardial tissue area, expressed as a percentage.
 (J and K) Representative M- and B-mode echocardiographic images from the PSLAX and SAX views. Images of the hearts were obtained before (baseline) and six weeks after injection with AAV-vector (J) or AAV1-*Scgb1a1*-OE (K).
 (L) LV ejection fraction (EF, %) at 0, 3, 6, 9, and 12 weeks after AAV injection. Statistical significance is determined by two-tailed unpaired Student's t tests. * $p < 0.05$, ** $p < 0.01$, *** $p < 0.001$, † $p < 0.0001$ vs. AAV-vector controls ($n = 8$ /group).

aberrant upregulation of SCGB1A1 in the hearts of male offspring and that cardiac SCGB1A1 overexpression alone is sufficient to induce pathological LV remodeling in male mice. These data position SCGB1A1 as a candidate, sex-dependent mediator of fPER-CCD-induced cardiac remodeling.

Using the same fPER-CCD protocol as described here, we previously reported that *in utero* CCD exposure affects depressive-like behaviors, hypothalamic protein expression, and pubertal onset and development in a sex-dependent manner.^{18,28} The present study extends our understanding of the long-term effects of fPER-CCD and reveals a heightened susceptibility of adolescent male offspring to pathological cardiac remodeling and cardiac arrhythmia. These male-biased effects are accompanied by more severe perturbations of circadian clock

gene expression in the hearts of male mice relative to females. Interestingly, although our previous study showed that fPER-CCD alters the amplitude but not the phase of molecular rhythms in the SCN,¹⁸ it appears to phase-advance the cardiac clock of male mice by several hours. This raises the possibility that CCD-F1-M mice suffer from internal desynchrony between the SCN and cardiac clocks, although further studies are needed to confirm the misalignment of SCN and cardiac rhythms in the same individuals.

Whether fPER-CCD-induced pathological cardiac remodeling is a consequence of circadian misalignment or heightened stress remains unclear. We previously showed that fPER-CCD increases the levels of plasma corticosterone in mice of both sexes.¹⁷ Others have demonstrated a similar effect on stress hormones when adult mice are subjected to chronic circadian misalignment.^{15,29} Given the reciprocal interactions between the circadian and stress systems, experimental approaches that can dissociate the two systems—whether surgical, pharmacological, or genetic—are needed to determine their individual contributions to fPER-CCD-induced cardiac remodeling.

Sex differences in cardiovascular disease (CVD) have been noted in both epidemiological and animal studies. Compared with women, men are diagnosed with CVD at a much younger age (by approximately 10 years), are more likely to have a heart attack, and have a lower life expectancy primarily as a consequence of ischemic heart disease.^{30,31} In mice, genetic perturbation of the circadian clock using the *Clock*^{Δ19} mutation results in the development of age-dependent cardiac hypertrophy in males but not females.¹¹ Interestingly, ovariectomized *Clock*^{Δ19/Δ19} female mice are similar to intact *Clock*^{Δ19/Δ19} males in developing dilated cardiomyopathy, indicating that female sex hormones exert a protective effect.⁶ Whether ovarian hormones also protect CCD-F1-F mice from pathological cardiac remodeling and tachyarrhythmia remains to be determined. Furthermore, given that we did not assess the effects of fPER-CCD on heart structure and function in mice older than eight weeks of age, we cannot exclude the possibility that female offspring may also experience pathological LV remodeling but with a later onset.

Our transcriptomic data revealed that fPER-CCD alters the expression of hundreds of genes in the heart, primarily in a sex-specific fashion. Such minimal overlap between the DEG datasets of male and female mice may explain why we did not observe cardiac remodeling in young females: despite other transcriptional perturbations, the key genes that trigger or mediate pathological LV remodeling might not be altered in female mice. In our study, we classified the DEGs as up- or downregulated based on evaluation of their expression at a single time point (~ZT 2). For genes that normally oscillate in their expression, it is quite possible that the observed differential expression is a reflection of a change in phase rather than in magnitude. However, in the case of *Scgb1a1*, *Scgb3a1*, and *Scgb3a2*, it seems unlikely that such massive increases in transcript abundance in CCD-F1 mice are due solely to altered phases of expression. A thorough examination of time-of-day-dependent expression of these and other DEGs will clarify whether the phase or magnitude of expression, or both, are altered.

Our data implicate SCGB1A1 as a potential mediator of fPER-CCD-induced cardiac remodeling. Not only does fPER-CCD robustly induce SCGB1A1 expression at the transcript and protein levels in male mice, but more importantly, cardiac overexpression of SCGB1A1 is sufficient to trigger myocardial hypertrophy in male mice that developed under normal conditions *in utero*. Whether SCGB1A1 overexpression can also induce cardiac remodeling in female mice remains to be examined. Future loss-of-function studies will address whether *Scgb1a1* is necessary for the LV remodeling phenotype in CCD-F1-M mice.

How SCGB1A1 might trigger pathological LV remodeling remains unclear. SCGB1A1 belongs to a large family of cytokine-like, SCGB proteins that are found in secretions of the lung, tear glands, salivary glands, prostate, and uterus.³² Originally discovered in rabbit endometrial fluid during early pregnancy, SCGB1A1 was later found in Clara cells of lung bronchioles and considered to be an early marker of lung injury.^{33,34} Previous studies have documented its expression in the heart and in transudates from patients with congestive heart failure.^{35,36} However, the function of SCGB1A1 within the heart remains obscure, with our study being the first, to our knowledge, to implicate its overexpression in pathological LV remodeling. On a different note, levels of serum SCGB1A1 exhibit moderate diurnal fluctuations, suggesting that SCGB1A1 may be clock-regulated. Future investigations are needed to establish the mechanistic links between the circadian clock, SCGB1A1 expression, and pathological LV remodeling. If *Scgb1a1* is indeed a clock-regulated gene, the resilience of the female cardiac clock to fPER-CCD-induced perturbation may, in part, explain why we did not observe pathological LV remodeling in young female mice.

Limitations of the study

1. An inherent limitation of our fPER-CCD protocol and similar chronic jetlag paradigms is the associated activation of stress mechanisms, as reflected in higher levels of stress hormones.^{37,38} The current study does not address the relative contributions of circadian and stress mechanisms to fPER-CCD-induced pathological cardiac remodeling.
2. Cardiac transcriptomes were profiled at a single time point, at ~ZT 2, in ISO-treated CCD-F1 and NC-F1 mice. Consequently, observed differences in gene expression may be due to a phase change in a rhythmic gene, an authentic up- or downregulation, or a combination of both. In addition, some DEGs may be ISO-induced immediate early genes that are impacted by fPER-CCD exposure. Further studies are required to exclude the effects of ISO treatment (e.g., by sampling from ISO-naïve mice) and to better characterize the changes in gene expression (e.g., sampling at multiple time points throughout the 24-h cycle).
3. The current study evaluated the effects of fPER-CCD on pathological cardiac remodeling in young (8-week-old) mice. A longitudinal study is required to determine whether female offspring are also susceptible to fPER-CCD-induced cardiac remodeling but at a later stage in life.

STAR★METHODS

Detailed methods are provided in the online version of this paper and include the following:

- KEY RESOURCES TABLE
- RESOURCE AVAILABILITY

- Lead contact
- Materials availability
- Data and code availability
- **EXPERIMENTAL MODEL AND STUDY PARTICIPANT DETAILS**
 - Mice
 - Experimental process
- **METHOD DETAILS**
 - Echocardiography
 - ECG
 - Glucose tolerance test
 - RNA-sequencing data quantification and analysis
 - Quantitative RT-PCR
 - Western blot analysis
 - Hematoxylin-eosin (H-E) and Sirius Red staining
 - Immunofluorescent staining
 - Enzyme-linked immunosorbent assays (ELISA)
 - Vector construction, AAV preparation and intramyocardial multi-points injection
- **QUANTIFICATION AND STATISTICAL ANALYSIS**

SUPPLEMENTAL INFORMATION

Supplemental information can be found online at <https://doi.org/10.1016/j.isci.2024.109008>.

ACKNOWLEDGMENTS

Peng Zhang was supported by Sichuan Province Science and Technology Support Program: NO. 2022YFS0607 (-B5), 2022YFS0610 (-A5), and 2024NSFSC0433 and The Southwest Medical University Support Program: NO. 2021ZKMS036. Wei-Chao Liu was supported by Sichuan Province Science and Technology Support Program: NO. 2021YFS0089 and Natural Science Program of Southwest Medical University: NO. 2020ZRZD008. Yang Yu was supported by Sichuan Province Science and Technology Support Program: NO. 2023NSFSC0593.

AUTHOR CONTRIBUTIONS

Conceptualization, P.Z.; methodology, Y.Y., J.Y.L., and P.Z.; formal analysis, W.C.L., and P.Z.; investigation, Y.Y., J.Y.L., H.J.Y., X.Q.L., X.P.G., X.X.H., and A.X.T.; writing—original draft, P.Z.; writing—review & editing, P.Z. and H.Y.M.C.; visualization, Y.Y., J.Y.L., and P.Z.; and funding acquisition, Y.Y., W.C.L., and P.Z.; resources, Y.Y. and P.Z.; supervision, W.C.L. and P.Z.

DECLARATION OF INTERESTS

The authors declare no competing interests.

Received: September 19, 2023

Revised: December 19, 2023

Accepted: January 22, 2024

Published: January 26, 2024

REFERENCES

1. Scheer, F.A.J.L., Hilton, M.F., Mantzoros, C.S., and Shea, S.A. (2009). Adverse metabolic and cardiovascular consequences of circadian misalignment. *Proc. Natl. Acad. Sci. USA* 106, 4453–4458. <https://doi.org/10.1073/pnas.0808180106>.
2. Muller, J.E., Stone, P.H., Turi, Z.G., Rutherford, J.D., Czeisler, C.A., Parker, C., Poole, W.K., Passamani, E., Roberts, R., Robertson, T., et al. (1985). Circadian variation in the frequency of onset of acute myocardial infarction. *N. Engl. J. Med.* 313, 1315–1322. <https://doi.org/10.1056/NEJM198511213132103>.
3. Martino, T.A., and Sole, M.J. (2009). Molecular time: an often overlooked dimension to cardiovascular disease. *Circ. Res.* 105, 1047–1061. <https://doi.org/10.1161/CIRCRESAHA.109.206201>.
4. Mistry, P., Duong, A., Kirshenbaum, L., and Martino, T.A. (2017). Cardiac clocks and preclinical translation. *Heart Fail. Clin.* 13, 657–672. <https://doi.org/10.1016/j.hfc.2017.05.002>.
5. Meléndez-Fernández, O.H., Walton, J.C., DeVries, A.C., and Nelson, R.J. (2021). Clocks, rhythms, sex, and hearts: How disrupted circadian rhythms, time-of-day, and sex influence cardiovascular health. *Biomolecules* 11, 883. <https://doi.org/10.3390/biom11060883>.
6. Alibhai, F.J., Reitz, C.J., Peppler, W.T., Basu, P., Sheppard, P., Choleris, E., Bakovic, M., and Martino, T.A. (2018). Female clock Δ 19/ Δ 19 mice are protected from the development of age-dependent cardiomyopathy. *Cardiovasc. Res.* 114, 259–271. <https://doi.org/10.1093/cvr/cvx185>.
7. Virag, J.A.I., and Lust, R.M. (2014). Circadian influences on myocardial infarction. *Front. Physiol.* 5, 422. <https://doi.org/10.3389/fphys.2014.00422>.
8. Khaper, N., Bailey, C.D.C., Ghugre, N.R., Reitz, C., Awosanmi, Z., Waines, R., and Martino, T.A. (2018). Implications of disturbances in circadian rhythms for cardiovascular health: A new frontier in free radical biology. *Free Radic. Biol. Med.* 119, 85–92. <https://doi.org/10.1016/j.freeradbiomed.2017.11.006>.
9. Zhou, L., Zhang, P., Cheng, Z., Hao, W., Wang, R., Fang, Q., and Cao, J.M. (2011). Altered circadian rhythm of cardiac

- β 3-adrenoceptor activity following myocardial infarction in the rat. *Basic Res. Cardiol.* 106, 37–50. <https://doi.org/10.1007/s00395-010-0110-7>.
- Crnko, S., Du Pré, B.C., Sluijter, J.P.G., and Van Laake, L.W. (2019). Circadian rhythms and the molecular clock in cardiovascular biology and disease. *Nat. Rev. Cardiol.* 16, 437–447. <https://doi.org/10.1038/s41569-019-0167-4>.
 - Alibhai, F.J., LaMarre, J., Reitz, C.J., Tsimakouridze, E.V., Kroetsch, J.T., Bolz, S.S., Shulman, A., Steinberg, S., Burris, T.P., Oudit, G.Y., and Martino, T.A. (2017). Disrupting the key circadian regulator CLOCK leads to age-dependent cardiovascular disease. *J. Mol. Cell. Cardiol.* 105, 24–37. <https://doi.org/10.1016/j.yjmcc.2017.01.008>.
 - Ingle, K.A., Kain, V., Goel, M., Prabhu, S.D., Young, M.E., and Halade, G.V. (2015). Cardiomyocyte-specific Bmal1 deletion in mice triggers diastolic dysfunction, extracellular matrix response, and impaired resolution of inflammation. *Am. J. Physiol. Heart Circ.* 309, H1827–H1836. <https://doi.org/10.1152/ajpheart.00608.2015>.
 - Anderson, S.T., and FitzGerald, G.A. (2020). Sexual dimorphism in body clocks. *Science* 369, 1164–1165. <https://doi.org/10.1126/science.abd4964>.
 - Morris, C.J., Purvis, T.E., Hu, K., and Scheer, F.A.J.L. (2016). Circadian misalignment increases cardiovascular disease risk factors in humans. *Proc. Natl. Acad. Sci. USA* 113, E1402–E1411. <https://doi.org/10.1073/pnas.1516953113>.
 - Thosar, S.S., Butler, M.P., and Shea, S.A. (2018). Role of the circadian system in cardiovascular disease. *J. Clin. Invest.* 128, 2157–2167. <https://doi.org/10.1172/JCI80590>.
 - Cao, N., Lan, C., Chen, C., Xu, Z., Luo, H., Zheng, S., Gong, X., Ren, H., Li, Z., Qu, S., et al. (2022). Prenatal Lipopolysaccharides Exposure Induces Transgenerational Inheritance of Hypertension. *Circulation* 146, 1082–1095. <https://doi.org/10.1161/CIRCULATIONAHA.122.059891>.
 - Zhang, P., Li, G., Li, H., Tan, X., and Cheng, H.Y.M. (2017). Environmental perturbation of the circadian clock during pregnancy leads to transgenerational mood disorder-like behaviors in mice. *Sci. Rep.* 7, 12641. <https://doi.org/10.1038/s41598-017-13067-y>.
 - Roth, G.A., Johnson, C., Abajobir, A., Abd-Allah, F., Abera, S.F., Abyu, G., Ahmed, M., Aksut, B., Alam, T., Alam, K., et al. (2017). Global, Regional, and National Burden of Cardiovascular Diseases for 10 Causes, 1990 to 2015. *J. Am. Coll. Cardiol.* 70, 1–25. <https://doi.org/10.1016/j.jacc.2017.04.052>.
 - Kessler, E.L., Rivaud, M.R., Vos, M.A., and van Veen, T.A.B. (2019). Sex-specific influence on cardiac structural remodeling and therapy in cardiovascular disease. *Biol. Sex Differ.* 10, 7. <https://doi.org/10.1186/s13293-019-0223-0>.
 - Shufelt, C.L., Pacheco, C., Tweet, M.S., and Miller, V.M. (2018). Sex-Specific Physiology and Cardiovascular Disease. *Adv. Exp. Med. Biol.* 1065, 433–454. https://doi.org/10.1007/978-3-319-77932-4_27.
 - Holdcroft, A. (2007). Gender bias in research: how does it affect evidence based medicine? *J. R. Soc. Med.* 100, 2–3. <https://doi.org/10.1177/014107680710000102>.
 - Blum, A., and Blum, N. (2009). Coronary artery disease: Are men and women created equal? *Gend. Med.* 6, 410–418. <https://doi.org/10.1016/j.genm.2009.09.005>.
 - Murphy, E. (2011). Estrogen signaling and cardiovascular disease. *Circ. Res.* 109, 687–696. <https://doi.org/10.1161/CIRCRESAHA.110.236687>.
 - Rossouw, J.E., Anderson, G.L., Prentice, R.L., LaCroix, A.Z., Kooperberg, C., Stefanick, M.L., Jackson, R.D., Beresford, S.A.A., Howard, B.V., Johnson, K.C., et al. (2002). Risks and benefits of estrogen plus progestin in healthy postmenopausal women: Principal results from the women's health initiative randomized controlled trial. *JAMA* 288, 321–333. <https://doi.org/10.1001/jama.288.3.321>.
 - Crosby, P., Hamnett, R., Putker, M., Hoyle, N.P., Reed, M., Karam, C.J., Maywood, E.S., Stangherlin, A., Chesham, J.E., Hayter, E.A., et al. (2019). Insulin/IGF-1 drives PERIOD synthesis to entrain circadian rhythms with feeding time. *Cell* 177, 896–909.e20. <https://doi.org/10.1016/j.cell.2019.02.017>.
 - Szántóová, K., Zeman, M., Veselá, A., and Herichová, I. (2011). Effect of phase delay lighting rotation schedule on daily expression of *per2*, *bmal1*, *rev-erb α* , *ppar α* , and *pd4* genes in the heart and liver of Wistar rats. *Mol. Cell. Biochem.* 348, 53–60. <https://doi.org/10.1007/s11010-010-0636-x>.
 - Zeman, M., Molcan, L., Herichova, I., and Okuliarova, M. (2016). Endocrine and cardiovascular rhythms differentially adapt to chronic phase-delay shifts in rats. *Chronobiol. Int.* 33, 1148–1160. <https://doi.org/10.1080/07420528.2016.1203332>.
 - Xu, L.N., Li, H.T., Liu, S., Jiang, J., Liu, Y.Q., Cheng, H.Y.M., Yu, Y., Cao, J.M., and Zhang, P. (2022). Constitutional delay of growth and puberty in female mice is induced by circadian rhythm disruption in utero. *Ecotoxicol. Environ. Saf.* 241, 113723. <https://doi.org/10.1016/j.ecoenv.2022.113723>.
 - Wright, K.P., Jr., Drake, A.L., Frey, D.J., Fleshner, M., Desouza, C.A., Gronfier, C., and Czeisler, C.A. (2015). Influence of sleep deprivation and circadian misalignment on cortisol, inflammatory markers, and cytokine balance. *Brain Behav. Immun.* 47, 24–34. <https://doi.org/10.1016/j.bbi.2015.01.004>.
 - Roth, G.A., Mensah, G.A., and Fuster, Valentin. (2020). The Global Burden of Cardiovascular Diseases and Risks: A Compass for Global Action. *J. Am. Coll. Cardiol.* 76, 2980–2981. <https://doi.org/10.1016/j.jacc.2020.11.021>.
 - Andersson, C., and Vasan, R.S. (2018). Epidemiology of cardiovascular disease in young individuals. *Nat. Rev. Cardiol.* 15, 230–240. <https://doi.org/10.1038/nrcardio.2017.154>.
 - Naizhen, X., Kido, T., Yokoyama, S., Linnoila, R.I., and Kimura, S. (2019). Spatiotemporal expression of three secretoglobin proteins, SCGB1A1, SCGB3A1, and SCGB3A2, in mouse airway epithelia. *J. Histochem. Cytochem.* 67, 453–463. <https://doi.org/10.1369/0022155419829050>.
 - Mukherjee, A.B., Zhang, Z., and Chilton, B.S. (2007). Uteroglobin: a steroid-inducible immunomodulatory protein that founded the Secretoglobin superfamily. *Endocr. Rev.* 28, 707–725. <https://doi.org/10.1210/er.2007-0018>.
 - Li, P., Li, Y., Zhang, J., Yu, S.F., Tong, W., Hu, X., and Jia, G. (2015). Biomarkers for lung epithelium injury in occupational hexavalent chromium-exposed workers. *J. Occup. Environ. Med.* 57, e45–50. <https://doi.org/10.1097/JOM.0000000000000436>.
 - Porter, D., Lahti-Domenici, J., Torres-Arzayus, M., Chin, L., and Polyak, K. (2002). Expression of high in normal-1 (HIN-1) and uteroglobin related protein-1 (UGRP-1) in adult and developing tissues. *Mech. Dev.* 114, 201–204. [https://doi.org/10.1016/s0925-4773\(02\)00056-4](https://doi.org/10.1016/s0925-4773(02)00056-4).
 - Hermans, C., Lesur, O., Weynand, B., Pieters, T., Lambert, M., and Bernard, A. (1998). Clara cell protein (CC16) in pleural fluids: a marker of leakage through the visceral pleura. *Am. J. Respir. Crit. Care Med.* 157, 962–969. <https://doi.org/10.1164/ajrccm.157.3.9707138>.
 - Golding, H., Ritonja, J.A., Day, A.G., Aronson, K.J., and Tranmer, J. (2022). Modeling the relationship between shift work and cardiometabolic risk through circadian disruption, sleep and stress pathways. *Chronobiol. Int.* 39, 704–713. <https://doi.org/10.1080/07420528.2022.2032124>.
 - Colwell, C.S. (2021). Defining circadian disruption in neurodegenerative disorders. *J. Clin. Invest.* 131, e148288. <https://doi.org/10.1172/JCI148288>.
 - Curtis, M.J., Hancox, J.C., Farkas, A., Wainwright, C.L., Stables, C.L., Saint, D.A., Clements-Jewery, H., Lambiase, P.D., Billman, G.E., Janse, M.J., et al. (2013). The Lambeth Conventions (II): guidelines for the study of animal and human ventricular and supraventricular arrhythmias. *Pharmacol. Ther.* 139, 213–248. <https://doi.org/10.1016/j.pharmthera.2013.04.008>.
 - Trapnell, C., Pachter, L., and Salzberg, S.L. (2009). TopHat: discovering splice junctions with RNA-Seq. *Bioinformatics* 25, 1105–1111. <https://doi.org/10.1093/bioinformatics/btp120>.
 - Trapnell, C., Williams, B.A., Pertea, G., Mortazavi, A., Kwan, G., van Baren, M.J., Salzberg, S.L., Wold, B.J., and Pachter, L. (2010). Transcript assembly and quantification by RNA-Seq reveals unannotated transcripts and isoform switching during cell differentiation. *Nat. Biotechnol.* 28, 511–515. <https://doi.org/10.1038/nbt.1621>.
 - Cornelissen, G. (2021). Applications of cosinor rhythmometry in pharmacology. *J. Pharmacokinet. Pharmacodyn.* 48, 339–359. <https://doi.org/10.1007/s10928-021-09748-x>.
 - Greenhouse, J.B., Kass, R.E., and Tsay, R.S. (1987). Fitting nonlinear models with ARMA errors to biological rhythm data. *Stat. Med.* 6, 167–183. <https://doi.org/10.1002/sim.4780060209>.
 - Refinetti, R., Lissen, G.C., and Halberg, F. (2007). Procedures for numerical analysis of circadian rhythms. *Biol. Rhythm Res.* 38, 275–325. <https://doi.org/10.1080/09291010600903692>.

STAR★METHODS

KEY RESOURCES TABLE

REAGENT or RESOURCE	SOURCE	IDENTIFIER
Antibodies		
Rabbit monoclonal Anti-Uteroglobin	Abcam	Cat# ab213203; RRID:AB_2650558
Goat polyclonal Anti-Mouse HIN-1/Secretoglobulin 3A1	R and D Systems	Cat# AF2954; RRID:AB_2157011
Rat monoclonal Anti-Mouse UGRP1/SCGB3A2 (IgG2B Clone # 381707)	R and D Systems	Cat# MAB3465
Rabbit polyclonal Anti-TH (H-196)	Santa Cruz Biotechnology	Cat# sc-14007
Mouse monoclonal Anti-MMP2 (101)	Thermo Fisher Scientific	Cat# 436000; RRID:AB_2532214
Rabbit polyclonal Anti-Collagen III	Thermo Fisher Scientific	Cat# PA5-34787; RRID:AB_2552139
Mouse monoclonal Anti-Sarcomeric Alpha Actinin	Abcam	Cat# ab9465; RRID:AB_307264
Rabbit recombinant monoclonal Anti-TNF alpha	Abcam	Cat# ab183218; RRID:AB_2889388
Rabbit monoclonal Anti-GAPDH (14C10)	Cell Signaling Technology	Cat# 5014 (also 5014S); RRID:AB_10693448
Mouse monoclonal Anti-beta Actin	Thermo Fisher Scientific	Cat# MA1-140; RRID:AB_2536844
Alexa Fluor 488 Donkey Anti-Goat IgG (H + L)	Abcam	Cat# ab150129; RRID:AB_2687506
Alexa Fluor 647 Donkey Anti-Mouse IgG (H + L)	Abcam	Cat# ab150107; RRID:AB_2890037
Goat polyclonal secondary Anti-rabbit IgG, HRP-linked Antibody	Cell Signaling Technology	Cat# 7074 (also 7074S, 7074V, 7074P2); RRID:AB_2099233
Horse polyclonal secondary Anti-mouse IgG, HRP-linked Antibody	Cell Signaling Technology	Cat# 7076 (also 7076S, 7076V, 7076P2); RRID:AB_330924
Anti-DDDDK tag (FLAG)	Abcam	Cat# ab205606; RRID:AB_2916341
Bacterial and virus strains		
AAV2-cTnt-Scgb1a1-3xflag-mCherry	Hanbio Biotechnology, Shanghai, CO. China	This paper
AAV2-cTnt-mCherry	Hanbio Biotechnology, Shanghai, CO. China	This paper
Chemicals, peptides, and recombinant proteins		
Paraformaldehyde	Sigma-Aldrich	Cat# 441244
Isoflurane	RWD (China)	Cat# R510-1
D-(+)-Glucose	Sigma-Aldrich	Cat# G8270
Isoprenaline hydrochloride	Sigma-Aldrich	Cat# BP205
NucleoZOL	Macherey-Nagel	Cat# 740404.200
Pierce RIPA buffer	Thermo Fisher Scientific	Cat# 89900
Donkey serum	Solarbio	Cat# SL050
Triton X-100 solution	Sigma-Aldrich	Cat# 93443
Sirius Red	Solarbio	Cat# G1470
Fade Fluorescence Mounting Medium containing DAPI	HelixGen	Cat# HNF0-02
Critical commercial assays		
BCA Protein Assay Kit	Thermo Fisher Scientific	Cat# 23225
ECL Detection Kit	Thermo Fisher Scientific	Cat# 32106
TransScript First-Strand cDNA Synthesis Super Mix Kit	Takara	Cat# RR047A
PowerUp SYBR Green master mix	Thermo Fisher Scientific	Cat# A25742
Mouse estradiol (E2) ELISA test Kit	Biovision	Cat# K3830-100
Testosterone (Testo) ELISA test Kit	Cloud-Clone	Cat# CEA458Ge
Mouse Brain Natriuretic Peptide (BNP) ELISA test Kit	Cloud-Clone	Cat# SEA541Mu

(Continued on next page)

Continued

REAGENT or RESOURCE	SOURCE	IDENTIFIER
Mouse N-Terminal Pro-Brain Natriuretic Peptide (NT-ProBNP) ELISA test Kit	Cloud-Clone	Cat# SEA485Mu
Mouse Tumor Necrosis Factor Alpha (TNF- α) ELISA test Kit	Cloud-Clone	Cat# SCA133Mu
Deposited data		
Raw data	This paper	PRJNA802082
Experimental models: Organisms/strains		
Mouse: C57BL/6J	The Jackson Laboratory	RRID: IMSR_JAX:000664
Oligonucleotides		
See Table S1 for primer sequences	This paper	N/A
AAV-m-Scgb1a1-Kpn/Kpn-F: ACCGCTCCGTGGGACGATCCC CGAGGATCCGCCACCATGAAGAT	This paper	N/A
AAV-m-Scgb1a1-Kpn/Kpn-R: TCCTCGCCCTTGCTCACCATGG TGGCAGGGCCGGGATTCTCTCCAC	This paper	N/A
Software and algorithms		
ImageJ (v8.0.0)	Schneider et al. ⁷	https://imagej.nih.gov/ij/
SAS version 9.4	SAS Institute, Cary, NC, USA	https://support.sas.com/kb/49/496.html
GraphPad Prism 9.5.0 (v1.0)	GraphPad Software	https://www.graphpad.com/
BL-420S system software (v2.0.0.3)	TECHMAN, Chengdu, China	N/A
cellSens	OLYMPUS	N/A
Photoshop	Adobe	N/A

RESOURCE AVAILABILITY**Lead contact**

Further information and requests for resources and reagents should be directed to and will be fulfilled by the lead contact, Peng Zhang (zhangpeng@swmu.edu.cn).

Materials availability

Materials generated in this study are available from the [lead contact](#)'s laboratory upon request.

Data and code availability

- All data reported in this paper will be shared by the [lead contact](#) upon request (zhangpeng@swmu.edu.cn).
- This paper does not report original code.
- Any additional information required to reanalyze the data reported in this paper is available from the [lead contact](#) upon request.

EXPERIMENTAL MODEL AND STUDY PARTICIPANT DETAILS**Mice**

All animal experiments were approved by the Institutional Care and Ethical Committee of Southwest Medical University (NO.:20191110-008; Luzhou, China), and were conducted in compliance with the *Guidelines for the Care and Use of Laboratory Animals* (National Institutes of Health, Bethesda, MD, USA). Animals were housed under a 12:12 h light/dark cycle (light intensity of 200 lux; lights on at 8:00 am, lights off at 8:00 pm) at an ambient temperature of $23 \pm 2^\circ\text{C}$. Regular rodent chow and water were provided *ad libitum*.

fPER-CCD-F1 mice were generated as described below. Eight-week-old, nulliparous F0 female mice were housed with age-matched male mice in a 2:1 ratio from 8:00 pm to 8:00 am of the next morning. Female mice were then checked for the presence of a vaginal plug. Plugged (i.e., pregnant) females were housed individually from the day that the plug was observed (considered as day 0 of gestation, or G0) to the day of birth (postnatal day 0, or P0), 18 to 21 days later. Pregnant mice were randomly divided into two groups (CCD or NC) according to treatment. The NC group ($n=20$) was maintained under normal, non-stressed conditions throughout the gestational period. The CCD group ($n=20$) was subjected to CCD from G0 to P0. The CCD paradigm involved delaying the 12:12 LD cycle by 8 hours every two days, achieved by extending the D phase by 8 hours.^{25,26} Light intensity in the L phase was set at 200 lux. Following delivery, P0 mice and the dam were returned to,

or maintained under, a fixed 12:12 LD schedule. Mice were weaned at P21 and divided into the following groups: NC-F1 male (NC-F1-M), NC-F1 female (NC-F1-F), CCD-F1 male (CCD-F1-M), and CCD-F1 female (CCD-F1-F).

Experimental process

Body weight (BW) was measured once weekly from 3 to 8 weeks of age. Echocardiography recordings were performed at 4, 6 and 8 weeks of age. Glucose tolerance and gonadal hormones were examined in 8-week-old mice. ISO-induced arrhythmia was assessed in 8-week-old mice by electrocardiogram (ECG) recording. Serum and tissues were collected immediately after ISO-induced cardiac arrest and death or once the ECG ended (in the surviving mice). These mice were anesthetized with isoflurane (~1.5%) and killed by cervical dislocation. Tissues were harvested between ZT 1 and ZT 2 and used for RNA-Seq, qRT-PCR, immunofluorescence staining, and Western blot analysis (Figure 1A).

METHOD DETAILS

Echocardiography

Transthoracic echocardiography was performed on anesthetized mice using a Vevo 3100 system (Fujifilm Visual Sonics, Toronto, ON, Canada) and a 30 MHz sectorial probe. Mice were anesthetized with 1% isoflurane mixed with 0.5-1.0 L/min air. Briefly, heart images were captured in the two-dimensional mode in the parasternal short-axis (SAX) and long-axis view (PLAX). M-mode tracings were recorded at the papillary muscle level and the left ventricular (LV) internal dimensions at diastole (LVIDd) and systole (LVIDs), as well as the LV posterior wall dimensions at diastole (LVPWd) and systole (LVPWs), were measured. The LV fractional shortening (FS, %) was calculated as $[(LVIDd - LVIDs)/LVIDd] \times 100$, and the LV ejection fraction (EF, %) was calculated as $[(LVIDd2 - LVIDs2)/LVIDd2] \times 100$. Echocardiography and downstream data analyses were conducted by the double-blind approach.

ECG

To record the surface ECG *in vivo*, mice were anesthetized with 1% isoflurane. A total of five recording electrodes were attached to the forelimbs, hind limbs and precordial region. ECG was recorded to monitor heart rate and rhythm with a computer-assisted BL-420S system (TECHMAN, Chengdu, China) with a sample rate of 1,000 Hz. Analysis was performed using the BL-420S system software (v2.0.0.3). Recordings were performed from ZT 1 to ZT 2. Baseline was recorded for 10 min, and recording was continued for 60 min after intraperitoneal (i.p) administration of isoprenaline hydrochloride (ISO) (51-30-9, Sigma-Aldrich), terminating earlier only upon death of the subject. Two doses of ISO, 10 and 100 $\mu\text{g}/\text{kg}$ (body weight), were used to successfully elicit tachyarrhythmia. Arrhythmias were compared with baseline ECGs exhibiting normal sinus rhythms. Arrhythmias were classified according to type based on the Lambeth Convention II.³⁹

Glucose tolerance test

After 12 h of fasting, mice were given 2 g/kg (body weight) glucose i.p at ZT6. Blood glucose concentrations following glucose challenge were determined by tail vein sampling at baseline and at 15, 30, 45, 60, 90, and 120 min after glucose injection using a hand-held glucometer (FreeStyle Lite, Abbott).

RNA-sequencing data quantification and analysis

For transcriptomic analysis, heart tissues were harvested from 8-week-old mice at the end of the ECG recording session. CCD-F1-M and CCD-F1-F mice that exhibited severe arrhythmic events (i.e., AVB, VT, VF) in response to high-dose ISO, and same-treated NC-F1-M and NC-F1-F mice that exhibited normal sinus rhythms, were selected for RNA-seq analysis. The RNA-Seq data from the Illumina BodyMap 2.0 project was generated by Illumina HiSeq 2500 with 150 bp paired-end sequencing. For each sample, ~40 million reads were generated. The Q30 base percentage of all samples was greater than 90.47%. We used Tophat⁴⁰ to map short reads onto the reference genome sequence of Mouse genome 38 (Mus_musculus.GRCm38.dna.toplevel.REF.fa). The mapped short reads were further processed to assemble transcripts and quantify transcript levels using Cufflinks.⁴¹ Transcript levels were quantified as Fragments Per Kilobase of exon per Million fragments mapped (FPKM). FPKM values were logarithm transformed for further analysis. Quantile-quantile (QQ) plots between tissues were drawn by R statistical programming language. DEGs were identified using the cuffdiff tool within Cufflinks package. DEGs were defined as those in which the log₂ Fold Change (FC) relative to NC controls was ≥ 1 or ≤ -1 , and the $-\log_{10}$ (P-value) was > 1.3 (i.e., $p < 0.05$) (Table S1). DEGs were annotated, analyzed, and visualized using the Metascape online analysis software (<https://metascape.org/gp/index.html#/main/step1>). The raw clean data have been deposited to Genbank (U.S. National Center for Biotechnology Information) under Sequence Read Archive accession number PRJNA802082.

Quantitative RT-PCR

Total RNA from heart and lung tissues were extracted with NucleoZOL reagent according to the manufacturer's instructions, and quantified using a spectrophotometer at 260 nm. The quality was evaluated based on the A260/A280 and A260/A230 ratios (NanoDrop 2000, Thermo Fisher Scientific). For each sample, 2 μg of total RNA was treated with gDNA wiper mix (RR047A, Takara) to remove any remaining genomic DNA, and reverse transcribed using the TransScript First-Strand cDNA Synthesis Super Mix Kit (RR047A, Takara) according to the manufacturer's instructions. Quantitative PCR was performed on a QuantStudio 5 Real-Time PCR System (Applied Biosystems) using PowerUp SYBR

Green master mix (A25742, Thermo Fisher Scientific) and gene-specific primers (Table S1). The expression of each gene was normalized to the internal control, *Gapdh*, and calculated using the $2^{-\Delta\Delta Ct}$ method.

Western blot analysis

Heart and lung tissues were lysed in Pierce RIPA buffer supplemented with Halt protease inhibitor cocktail. Lysates were centrifuged at 12,000 rpm for 20 min at 4°C, and the supernatants were analyzed using the BCA Protein Assay Kit to quantify protein concentration. Proteins (20 µg/well) were resolved by electrophoresis on a 4%-12% SurePAGE gel (M00652, Genscript), and were subsequently transferred to PVDF membranes (Merck Millipore). The membrane was blocked with TBST (Tris buffered saline with 0.1% Triton X-100) solution containing 5% skim milk and incubated overnight at 4°C with a target-specific primary antibody (Table S2). After washing in TBST, membranes were incubated with horseradish peroxidase-conjugated anti-rabbit or anti-mouse secondary antibodies for 2h at room temperature (RT). Blots were developed using an ECL Detection Kit (32106, Thermo Fisher Scientific), and chemiluminescence images were captured using Universal Hood II (Bio-Rad). Relative protein abundance was quantified using the ImageJ software (v8.0.0), based on previously described methods (Bass et al). Values are presented as fold-change of the protein normalized to relative abundance of GAPDH (n = 3 mice/group). The uncropped blot is shown in Figure S6.

Hematoxylin-eosin (H-E) and Sirius Red staining

Paraffin-embedded hearts were sectioned along the long axis to obtain 4-µm-thick slices. Routine H-E staining was performed to visualize the overall morphology and structure of cardiac walls and chambers. To assess collagen deposition, three paraffin sections were randomly selected for each heart and stained with Sirius Red according to the manufacturer's instructions. The percentage of red-stained area versus the total area was determined and used as an index of collagen density (i.e., fibrosis). Data analysis was performed with ImageJ. For each group, a total of 5 animals were examined.

Immunofluorescent staining

Hearts were sectioned on a cryostat to obtain 10-µm-thick coronal sections. Immunofluorescent staining was used to detect the expression of collagen type III alpha 1 (COL3A1) and α -ACTIN. For immunofluorescence, tissue sections were washed 5 × 5 min in phosphate buffered saline with 0.1% Triton X-100 (PBST). Sections were blocked with 10% goat serum or 10% horse serum in PBST at RT for 1h and incubated overnight at 4°C with primary antibodies (Table S2). The following day, tissue sections were washed 5 × 5 min in PBST at RT. Tissues were incubated with Alexa Fluor 488 donkey anti-goat IgG H&L and Alexa Fluor 647 donkey anti-mouse IgG H&L secondary antibodies for 2h in the dark at RT. After 5 × 5 min washes in PBST, tissues were mounted and the slides were cover-slipped with Anti-Fade Fluorescence Mounting Medium containing DAPI and sealed with nail polish. Images were acquired on an Olympus BX63 fluorescence microscope. Immunopositive areas were quantified using Image J.

Enzyme-linked immunosorbent assays (ELISA)

Blood samples were collected from the tail vein or right ventricle, and sera were separated by centrifugation at 3,000 rpm for 25 minutes at RT. Commercial ELISA kits were used to measure the serum levels of hormones or cytokines, including estradiol (E2), testosterone (Testo), Brain Natriuretic Peptide (BNP), N-Terminal Pro-Brain Natriuretic Peptide (NT-ProBNP), and Tumor Necrosis Factor Alpha (TNF- α).

Vector construction, AAV preparation and intramyocardial multi-points injection

The AAV2-cTNT-*Scgb1a1*-3xflag-mCherry (AAV-*Scgb1a1*) and the control AAV-cTNT-mCherry vectors were purchased from Hanbio Biotechnology (Shanghai, CO. China). The sequences of primers used to amplify full-length *scgb1a1* are provided in the Key resources table of STAR Methods. Briefly, AAV packaging was accomplished by transfecting HEK293T cells with AAV-*Scgb1a1* or control AAV vector along with pAAV-9 and pHelper. Seventy-two hours post-transfection, cells were collected, lysed and loaded onto an iodixanol gradient for centrifugation at 400,000 ×g for 2 hr. To remove residual plasmid and 293T genomic DNA, Benzonase nuclease (9025-65-4, Millipore) was added to the crude viral extract at 0.1 µl per 1 mL of extract, and incubated for 1 hr at 37°C prior to centrifugation at 600 ×g or 10 min at 4°C. AAV particles were purified and concentrated using the AAV Purification Maxiprep Kit (V1469-01, Biomiga). Infectious titers were measured by infecting HEK293T cells and determined to be 2.0×10^{12} vg/ml for AAV- *Scgb1a1* and 1.8×10^{12} vg/ml for control AAV.

Six-week-old C57BL/6J mice were anesthetized, intubated and ventilated using a rodent ventilator R500 system. The heart was exposed by thoracotomy and injected intramyocardially with AAV-*Scgb1a1* or control AAV at 5 different sites (10µl/site) in the left ventricle. The chest was sutured and the animal was given an intramuscular injection of penicillin (80,000 U). Cardiac function was measured by echocardiography at 0, 3-, 6-, 9-, and 12-weeks post-surgery.

QUANTIFICATION AND STATISTICAL ANALYSIS

The expression profiles of circadian clock genes were evaluated by the *Cosinor analysis* method using mixed model analyses of variance (PROC MIXED) with SAS version 9.4 (SAS Institute, Cary, NC, USA). The *Cosinor analysis* uses a pair of ~24-h sine and ~24-h cosine curves to identify a "circadian effect" (a fundamental circadian component of ~24-h). These analyses applied cosinor mixed model analyses for

biorhythmic data based on fitting a circadian rhythm with a series of sine and cosine curves, including autoregressive error structures to model the strong serial correlation often seen in biorhythmic data.^{42–44}

In addition, all quantitative data are expressed as mean \pm standard deviation (SD). Statistical analyses were performed using GraphPad Prism 9.5.0 (v1.0). Two-tailed unpaired Student's t-tests ($n \geq 5$ per group) or Mann–Whitney tests ($n < 5$ per group) were used to compare the two groups. Two-way ANOVAs were used to analyze two groups and ≥ 2 time points/treatments. Prior to the use of parametric statistics, we ensured that the data were normally distributed using the Shapiro-Wilk test. The X^2 test was used to analyze the frequency of arrhythmic events between groups. Survival distributions were compared by the log-rank (Mantel-Cox) test. For all tests, $p < 0.05$ (*) was considered statistically significant.